FLASH*lab*@PITZ: New R&D platform with unique capabilities for electron FLASH and VHEE radiation therapy and radiation biology under preparation at PITZ

Frank Stephan [a,*], Matthias Gross [a], Anna Grebinyk [a], Zakaria Aboulbanine [a,c], Zohrab Amirkhanyan [a,d], Volker Budach [e], Vincent Henrique Ehrhardt [f], Angeles Faus-Golfe [g], Marcus Frohme [b], Jean-Francois Germond [h], James David Good [a], Florian Grüner [i], David Kaul [e], Mikhail Krasilnikov [a], Ron Leavitt [j], Wim Leemans [k], Xiangkun Li [a], Gregor Loisch [k], Frieder Müller [a], Georg Müller [l], Frank Obier [k], Anne Oppelt [a], Sebastian Philipp [a], Houjun Qian [a], Judith Reindl [m], Felix Riemer [a], Martin Sack [l], Michael Schmitz [k], Tobias Schnautz [k], Andreas Schüller [n], Theresa Staufer [i], Christian Stegmann [a], Gohar Tsakanova [o,p], Marie-Catherine Vozenin [j], Hans Weise [k], Steven Worm [a], Daniel Zips [e]

[a] *Deutsches Elektronen-Synchrotron DESY, Platanenallee 6, 15738 Zeuthen, Germany*
[b] *Technical University of Applied Sciences Wildau, Hochschulring 1, 15745 Wildau, Germany*
[c] *On Leave from University Mohammed V, Rabat, Morocco*
[d] *On Leave from CANDLE Synchrotron Research Institute, Yerevan, Armenia*
[e] *Department of Radiotherapy, Charité Berlin, CCM/CVK, 13353 Berlin, Germany*
[f] *University Medical Center Hamburg-Eppendorf, Martinistraße 52, 20251 Hamburg, Germany*
[g] *Laboratoire de Physique des 2 Infinies, Irene Joliot-Curie Laboratory IJCLab, CNRS/IN2P3, Universite Paris-Saclay, Orsay 91898, France*
[h] *CHUV, Institut de Radiophysique, Rue du Grand-Pré 1, CH-1007 Lausanne, Switzerland*
[i] *Universität Hamburg and Center for Free-Electron Laser Science, Luruper Chaussee 149, 22761 Hamburg, Germany*
[j] *CHUV, Service de Radio-Oncologie, Rue du Bugnon 46, CH-1011 Lausanne, Switzerland*
[k] *Deutsches Elektronen-Synchrotron DESY, Notkestr. 85, 22603 Hamburg, Germany*
[l] *Karlsruhe Institute of Technology (KIT), Institute for Pulsed Power and Microwave Technology (IHM), Hermann-von-Helmholtz-Platz 1, 76344 Eggenstein-Leopoldshafen, Germany*
[m] *Universität der Bundeswehr München, Werner-Heisenberg-Weg 39, 85577 Neubiberg, Germany*
[n] *Physikalisch-Technische Bundesanstalt (PTB), Bundesallee 100, Braunschweig 38116, Germany*
[o] *Institute of Molecular Biology NAS RA, Yerevan, Armenia*
[p] *CANDLE Synchrotron Research Institute, Yerevan, Armenia*

ARTICLE INFO

Keywords:
FLASH and VHEE radiation therapy
Ultra-high dose rate
Flexible electron accelerator
Online image guiding
Uniquely wide parameter range

ABSTRACT

At the **P**hoto **I**njector **T**est facility at DESY in **Z**euthen (PITZ), an R&D platform for electron FLASH and very high energy electron radiation therapy and radiation biology is being prepared (FLASH*lab*@PITZ). The beam parameters available at PITZ are worldwide unique. They are based on experiences from 20 + years of developing high brightness beam sources and an ultra-intensive THz light source demonstrator for ps scale electron bunches with up to 5 nC bunch charge at MHz repetition rate in bunch trains of up to 1 ms length, currently 22 MeV (upgrade to 250 MeV planned). Individual bunches can provide peak dose rates up to 10^{14} Gy/s, and 10 Gy can be delivered within picoseconds. Upon demand, each bunch of the bunch train can be guided to a different transverse location, so that either a "painting" with micro beams (comparable to pencil beam scanning in proton therapy) or a cumulative increase of absorbed dose, using a wide beam distribution, can be realized at the tumor. Full tumor treatment can hence be completed within 1 ms, mitigating organ movement issues. With extremely flexible beam manipulation capabilities, FLASH*lab*@PITZ will cover the current parameter range of successfully

* Corresponding author.
E-mail address: frank.stephan@desy.de (F. Stephan).

https://doi.org/10.1016/j.ejmp.2022.10.026
Received 24 April 2019; Received in revised form 30 May 2019; Accepted 31 May 2019

demonstrated FLASH effects and extend the parameter range towards yet unexploited short treatment times and high dose rates. A summary of the plans for FLASH𝒻𝒶𝓈𝓉@PITZ and the status of its realization will be presented.

1. Introduction

The classical approach of radiation therapy for cancer care relies largely on the rationale that cancer cells are less efficient in repairing DNA damages than normal cells – an effect that is also dependent on the tumor microenvironment [1]. However, radiation can damage normal tissue surrounding the treated tumor and radioresistance occurs [2–4] that limits the applied treatment dose and causes cancer relapse, respectively. The treatment of radiation-resistant and metastatic cancers is nowadays a major challenge. Therefore, it is of critical importance to widen the therapeutic window of radiation therapy, i.e. the differential effect between tumor tissue and normal tissue response, to be able to decrease side effects, while at least keeping tumor control. The novel field of FLASH radiation therapy (FLASH RT) – radiation at ultra-high dose rates (UHDR) with short treatment times that not only maintains anticancer action of conventional radiation therapy, but also reduces toxicities of normal surrounding tissue – is called the FLASH effect. FLASH RT allows new treatment regimen and can shorten the overall time for the optimum dose delivery by about several thousand times. This ultimately offers not only comfort to the patient but also economic advantages, reducing costs and curing more patients in the same amount of time.

Pioneering investigations in the late 1960s to 1970s already showed that UHDR radiation has a much smaller impact to normal tissue than conventional irradiation schemata [5–7]. But conversely to the common dogma, in 2014 Favaudon et al. showed that in addition to the strongly reduced impact on normal tissue, UHDR radiation was able to eradicate tumors in xenografted and orthotopic tumor-bearing mice [8]. The increase of the mean dose rate from conventional ($\leq$0.03 Gy/s) to ultra-high levels (40–60 Gy/s) reduced pulmonary fibrosis in mice. This sparked a flurry of activity, and the FLASH effect was demonstrated in several experimental animal models (mice, rat, zebrafish) and multiple organs (lung, skin, gut, brain, bone) [9–20]. The FLASH effect was demonstrated with electrons, protons and photons, but electrons were used in most cases, as also in the effort described in this paper. Therefore, electron FLASH RT is meant in the following if not stated otherwise. In parallel, efforts were started to explain the mechanism of the FLASH effect. A few reviews summarize the efforts so far [18,21–24], but due to persisting lack of clarity on the fundamentals of the FLASH effect the work on modeling and simulations is ongoing.

Overall one can state that detailed explanation of the observed effects, many crucial experiments and optimization of the FLASH RT for different tumor types are still missing. To address the lack of experimental data, dedicated efforts have started: for proton FLASH RT the technical challenges were addressed by Jolly et al. [25].

Utilizing electrons, besides modified commercial accelerator systems also research accelerators like for example CLEAR at CERN [26–28] and ELBE at HZDR [17,29] have been used for UHDR and FLASH RT studies in their specifically given parameter range. CLEAR can provide electron beams of up to 220 MeV with bunch charges of up to 3 nC and in total 75 nC within 100 ns at 10 Hz repetition rate [26]. ELBE allows beam energies up to 40 MeV with bunch charges of up to ~0.25 nC at varying repetition rates with a maximum average current of up to 1.6 mA [29].

In this paper we report about a collaborative effort, called FLASH𝒻𝒶𝓈𝓉@PITZ. This has recently started under the leadership of Deutsches Elektronen-Synchrotron (DESY) together with its local collaborator Technical University of Applied Sciences Wildau (TH Wildau) and several national and international partners to systematically study the conditions for FLASH RT. An electron FLASH RT R&D beamline will be installed at the existing research accelerator Photo Injector Test facility at DESY in Zeuthen (PITZ). This should allow gaining an in-depth understanding of the FLASH effect and optimizing the FLASH treatment beam parameters for different types of tumors, fully utilizing the capabilities of the PITZ facility. Currently electron beam energies of up to 22 MeV can be provided with bunch charges up to 5 nC and bunch train charges within 1 ms up to 5000 nC (upgrade by factor 4.5 to be realized in 2023). These parameters for UHDR irradiation allow to provide a worldwide uniquely wide parameter range for studying the FLASH effect, see Sections 2.2–2.4.

The FLASH effect is defined in a living organism and has to be demonstrated with animal experiments. Therefore, the planned work is organized in four work packages which are not sequential but overlappingly address different goals that are interdependent: the first work package is the preparation of biological experiments with beam dynamics simulation, dosimetry experiments and *in silico* predictions of FLASH effects. The second and third work package are *in vitro* experiments for preparing the subsequent *in vivo* studies, and the fourth work package is a beam energy upgrade from currently 22 MeV to up to 250 MeV. This will allow to optimize the dose delivery for FLASH RT treatment for different types of cancer, including deep-seated tumors. The ultimate goal is the definition of optimum beam parameters for clinical treatments of humans with very high energy electron (VHEE) FLASH RT.

The paper is organized that in the following Section 2 the PITZ infrastructure will be described, demonstrating the unique capabilities of the accelerator towards opening a new window in FLASH RT. In Section 3 a proposal to fully utilize the possibilities given and the different work packages being followed will be described. This comprises the main work of *in vitro* and *in vivo* experiments plus preparatory work for a possible facility extension towards higher beam energies. In Section 4 first results towards realization of FLASH𝒻𝒶𝓈𝓉@PITZ are described.

2. Description of the PITZ infrastructure

2.1. Basic principle of the electron source

The Photo Injector Test facility at DESY in Zeuthen (PITZ) was built for doing research and development on high brightness electron sources that are needed for super-conducting linear accelerator (linac) driven, high duty cycle, pulsed, short wavelength Free-Electron Lasers (FELs). Examples for this are the user facilities FLASH, the XUV and soft X-ray Free-Electron Laser Facility at DESY [30,31], and the European X-ray Free-Electron Laser (European XFEL) [32,33], both operated by DESY in Hamburg. For reaching the required beam quality, the electron bunches are produced in a 1.6-cell photo cathode radio frequency (RF) gun operated at a resonance frequency of 1.3 GHz with a high cathode gradient of up to 60 MV/m. More details can be found in [34]. The electrons then receive further acceleration by a booster cavity. Besides these key components a large number of additional instrumentations is available in the PITZ beamline for detailed control and diagnostics of the electron beam, see Fig. 1. After optimization the PITZ photo injector was able to demonstrate world leading beam quality in a wide range of electron bunch charges from 0.02 to 2 nC [35]. Other key issues of the photo injector are its stability and reliability [36]. As discussed in detail in this reference, the PITZ accelerator has several feedback loops to stabilize its water cooling system and RF power systems, resulting in stable bunch charge production and corresponding dose delivery. Fig. 2 shows examples of bunch charge measurement statistics (left) and bunch charge along a bunch train (right). Both measurements show relative errors in the sub percent level; 0.65 % and 0.56 %, respectively. These numbers already include noise from the electronic readout system. This

demonstrates the current stability on bunch charge and together with the available charge measurement devices, very good reproducibility of bunch charge is given. Further improvement on the bunch charge stability is expected with the new photo cathode laser system which is expected to be installed in 2023.

2.2. Unique time structure of the electron bunches

Since the PITZ electron source has to feed the super-conducting linacs of the FEL user facilities FLASH, the XUV and soft X-ray Free-Electron Laser Facility at DESY, and the European XFEL, it can offer a worldwide unique time structure of the electron bunches that can be generated. **The RF pulses in the RF gun can have a length of up to 1 ms and the repetition rate of these RF pulses currently can be chosen to be between 1 and 10 Hz.** The photo cathode laser systems available at PITZ currently allow laser pulse repetition rates from 100 kHz to 1 MHz so that **within the maximum length of the RF pulses of 1 ms currently up 1000 electron bunches can be produced as a bunch train sequence** (Fig. 3). With a laser upgrade to 4.5 MHz in 2023 even up to 4500 electron bunches will be possible within 1 ms.

2.3. Unique properties of the individual electron bunches

The number of electrons in each electron bunch (i.e. the bunch charge) can be adjusted by changing the laser intensity hitting the photo cathode. A lower bound on this parameter is only set by the capability of

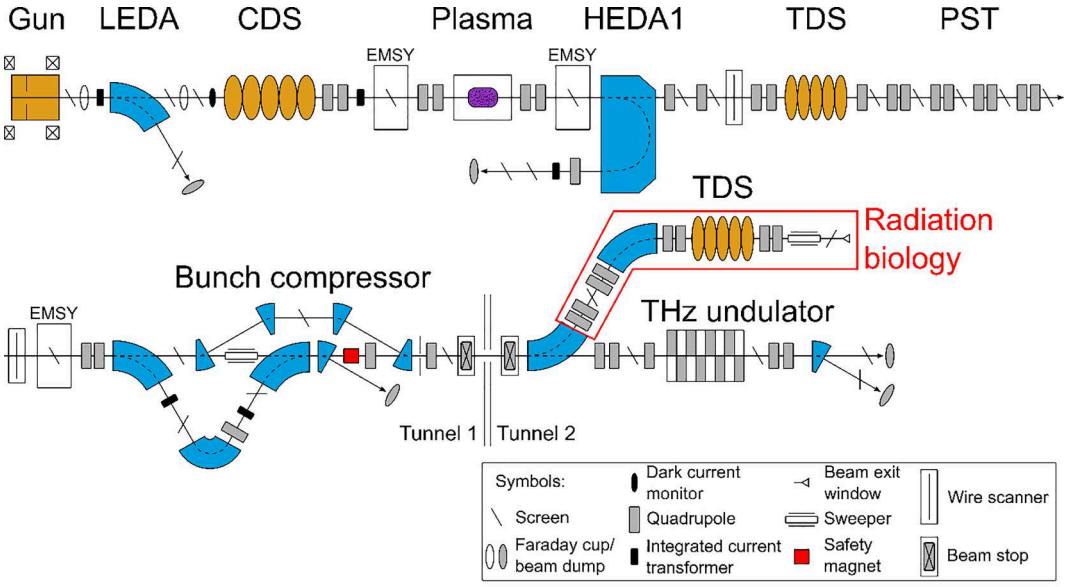

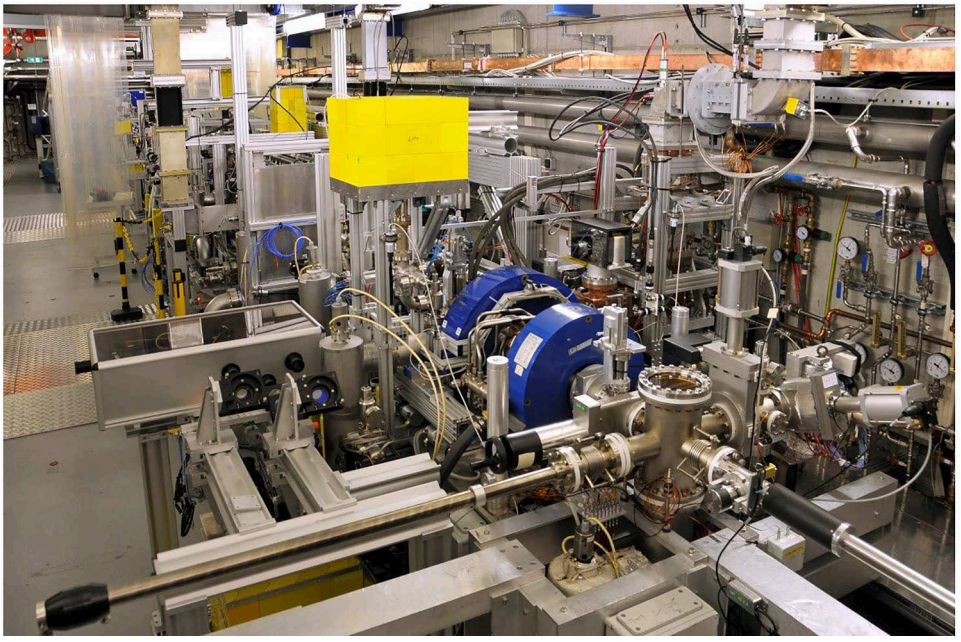

Fig. 1. Schematic and photograph of the PITZ accelerator. The upper part of the figure shows a schematic of the existing photo injector layout (split in two lines to be better readable). GUN – electron source, LEDA – low energy dispersive arm, CDS – cut disk structure booster cavity, Plasma – test area for e.g. plasma acceleration, HEDA1,2 – high energy dispersive arm 1 and 2, TDS – transverse deflecting structure, PST – phase space tomography section, EMSY – emittance measurement system. The part framed in red is the new R&D beamline for FLASH RT and radiation biology that is subject of this paper. The lower part of the figure shows a photograph of the RF gun section in tunnel 1. © 2022 Frank Stephan. (For interpretation of the references to color in this figure legend, the reader is referred to the web version of this article.)

detecting a clear signal of electrons above electronic noise. On the other hand there exists an upper bound for high bunch charges due to the space charge limit of photo emission. This is reached when the so-called longitudinal space charge field of the already emitted electrons over-compensates the accelerating RF field at the cathode so that no further electrons can be emitted. **Bunch charges over more than 5 orders of magnitude, in the charge range between 0.03 pC and 6000 pC, have been measured** with the existing setup. The high tuneability on the bunch charge allows an extremely flexible adjustment of the radiation dose that is deposited by the individual electron bunches.

Experimental studies at PITZ have been able to demonstrate electron bunch lengths from some hundred femtoseconds for low charges up to 30–40 ps for high charges. A bunch compressor recently installed will allow a larger tuning range of the bunch length so that **single bunch lengths in the range from 0.1 to 60 ps can be produced**, depending on the bunch charge. For a fixed bunch charge, changing the bunch length allows a flexible adjustment of the radiation dose rate while keeping the deposited dose constant.

For its original application as a high brightness electron source for short wavelength FELs, the PITZ photo injector has to deliver the best possible beam quality. Especially the transverse emittance, a measure of the product of transverse beam size and angular divergence of the electron beam, has to be as small as possible. This capability was demonstrated experimentally at PITZ [35] and is also beneficial for radiation applications: The electron beam is very well controlled and currently allows **electron spot sizes from a few centimeters down to about 100 µm**, dependent on the single bunch charge and beam energy. The large spot sizes allow full irradiation of a large tumor volume. The small spot sizes can not only increase the local dose that is deposited in a radiation volume but also allow generating narrow pencil beams. Such pencil beams together with the PITZ capability of generating bunch trains with currently up to 1000 bunches in 1 ms and a fast, pulsed magnetic system deflecting the electron beam (called kicker for single deflection or sweeper for 'painting' an area) will allow **scanning of up to 1000 electron bunches over the radiation area within a total treatment time of 1 ms!** Such a short treatment time will make it possible to neglect the organ motion during the radiation process assuming that the tumor location is monitored online (see Section 4.1). The beam spot size during this beam scanning can be either chosen such that partially overlapping beam profiles cause a homogeneous dose distribution, or spatially separated pencil beams hit the tumor area. In all cases the bunches are expected to fulfill the FLASH RT conditions. While the small spot size of this pencil beam scanning over the tumor

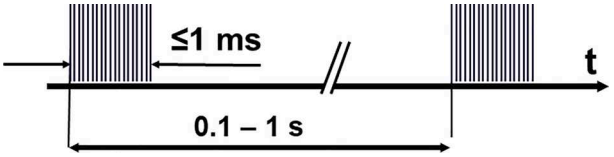

Fig. 3. The pulsed time structure of the electron bunches currently available at PITZ. The electron bunches at PITZ are produced in bunch trains, which can have a length of up to 1 ms. The bunches within these trains are currently repeated with 100 kHz to 1 MHz so that the separation of neighboring bunches is between 1 and 10 µs. The number of bunches in the bunch trains can be freely chosen from 1 to 1000 bunches (for 1 MHz bunch repetition rate). These trains of bunches can be repeated with 1–10 Hz so that the separation between neighboring bunch trains is between 0.1 and 1 s. Within the described limitations the bunch pattern can be freely chosen by user needs. © 2022 Frank Stephan.

Table 1
List of some key operation parameters of PITZ for two (extreme) cases. The bunch charge is the charge within a single electron bunch (i.e. within one RF cycle) and can be freely chosen. The user can also choose if a single bunch or a train of bunches is wanted. The RF pulses in which the single bunches or bunch trains are accelerated can have a length of up to 1 ms and can be repeated with a repetition rate between 1 and 10 Hz. The single bunch length is adjustable by laser shaping, RF phasing and the bunch compressor. The doses and dose rates are calculated per bunch (D_{bunch} and $\dot{D}_{bunch}$), per bunch train (i.e. within 1 ms, D_{train} and $\dot{D}_{train}$) and per second ($\langle\dot{D}\rangle$, average dose rate) depending on the parameters chosen in the upper lines of the table. For the dose and dose rate values the energy deposition of a 20 MeV electron beam over 1 mm depth in water and using a 1 mm^2 spot size was estimated.

Options @PITZ	Low dose case	High dose case
Bunch charge [pC]	0.1	5 000
Individual bunches OR train	Single bunch	1 ms train, (i.e.1000 bunches)
RF pulse rep. rate [Hz]	1	10
Bunch length [ps]	<1	~30
Dose (D_{bunch}) **per bunch** [Gy]	0.02	1000
Dose rate ($\dot{D}_{bunch}$) **per bunch** [Gy/s]	>2E+10	4E+13
Dose (D_{train}) **per train (ms)** [Gy]	0.02	1E+6
Dose rate ($\dot{D}_{train}$) **per train (ms)** [Gy/s]	20	1E+9
Dose **per second** ($\langle\dot{D}\rangle$) [Gy/s]	0.02	1E+7

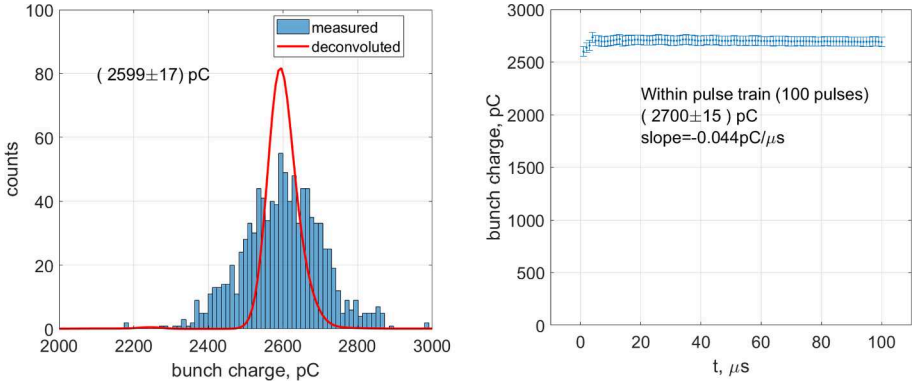

Fig. 2. Bunch charge measurements statistics (left) and bunch charge along a bunch train (right). Measurements were conducted at a bunch charge level which can be used for FLASH RT experiments at PITZ. The bunch charge statistics on the left shows the histogram of 1000 measurements of the first bunch in the bunch train (blue bars) and the distribution deconvoluted from the background noise (red curve). This resulted in a bunch charge of 2599 ± 17 pC. The charge along a pulse train with 100 pulses was 2700 ± 15 pC with a slope of −0.044 pC/µs, again with a statistic of 1000 measurements. Statistical errors are given for the measurements, both showing relative stability in the sub-% level. A new photo cathode system being installed in 2023 is expected to further improve the bunch charge stability. © 2022 Frank Stephan. (For interpretation of the references to color in this figure legend, the reader is referred to the web version of this article.)

area will be broadened by multiple scattering of the beam electrons in the vacuum exit window and in the tissue at low beam energy (the current PITZ facility it is limited to ~22 MeV), it would reach its full potential at high electron beam energies after an energy upgrade to 250 MeV at PITZ.

2.4. Unique R&D capabilities on radiation biology and FLASH RT at PITZ

Table 1 lists two (extreme) cases of PITZ operation parameter choices and shows the corresponding local doses and dose rates that can be deposited in the tissue.

By varying the PITZ operation parameters like bunch charge, single bunch or bunch train operation, single bunch repetition rate within the train, RF pulse repetition rate or length of the individual bunch, an extremely wide parameter range is accessible at PITZ. Fig. 4 shows this wide parameter range as a function of two parameters: on the vertical axis the time that is needed to deliver 10 Gy to a certain volume that has to be irradiated (a common value for a dose delivery session) and on the horizontal axis the dose rate during the delivery. On the horizontal axis one has to distinguish between 3 different estimates: a) the bunch or peak dose rate delivered within the individual electron bunches ($\dot{D}_{bunch}$), which is marked as red area, b) the average dose rate in the bunch train when more than 1 bunch is used in the train ($\dot{D}_{train}$), which is marked as blue area, and c) the total dose delivered over one second ($\langle\dot{D}\rangle$), which is marked as green area. The estimation in Fig. 4 again assumes the energy deposition of a 20 MeV electron beam over 1 mm depth in water and using a 1 mm^2 spot size, identical to the examples given in Table 1. The time to deliver 10 Gy is defined by the bunch charge and the bunch repetition rate. Since for this figure a single bunch repetition rate of 1 MHz was assumed, a gap in the time needed to deliver 10 Gy between about 1 μs and 60 ps is visible. This stems from the fact that either 2 bunches with a separation of 1 μs are needed to deliver 10 Gy or the 10 Gy are provided by a single bunch, which is stretched in length. This gap can be overcome e.g. by using a 1.3 GHz photo cathode laser system, which can fill a low charge bunch in every RF cycle of the 1 ms RF pulse. This option is also shown with the corresponding colors in the figure. The two operational cases listed in Table 1 are marked with a green circle for the low dose case and with a red circle for the high dose case in Fig. 4.

Also shown is published data for the conditions to obtain reproducible FLASH effects (fully filled markers in the center of the plot) and conditions which could not show the FLASH effect (marked with crosses in the plot), adapted from [14,37]. With this comparison one can clearly see that the enormously wide parameter range accessible at PITZ not only covers the recent state of the art of FLASH RT worldwide but also offers to study and exploit yet unexplored high dose rates and short delivery times. On the other hand, it additionally offers to emulate the study of conventional radiation therapy at the same facility as marked with a red star in the upper left part of the plot by using many low-charged bunches. Having this wide parameter range available at a single facility allows a direct comparison of optimized FLASH therapy results with conventional radiation therapy. Additionally, it should allow reducing the systematic uncertainties in these comparisons in contrast to having to compare experiments from different facilities.

3. Overview of the different R&D work packages of the FLASH*ology*@PITZ project

In the first work package, the basic version of the beam delivery system for FLASH RT radiation biology is designed, built and installed. Beam dynamics and dosimetry experiments are performed using corresponding detectors, phantoms and non-biological samples. Also, computer simulations following the whole irradiation chain from dosimetry, via *in vitro* and *in vivo* experiments with biological samples up to longer term medical effects of the delivered radiation will start in this work package and will continue and be refined over the entire project duration.

In the second work package, the *in vitro* experiments will use thin chemical and biological models like inorganic and organic molecules, cells and tissues etc. This is done not only to understand the effects of UHDR radiation on and interaction with inorganic, organic and living matter, but also to reduce the subsequent number of *in vivo* experiments.

Once the above described preparatory work for performing *in vivo* studies is completed, the third work package of the R&D program can start. Since the leading conception defines the FLASH effect as a

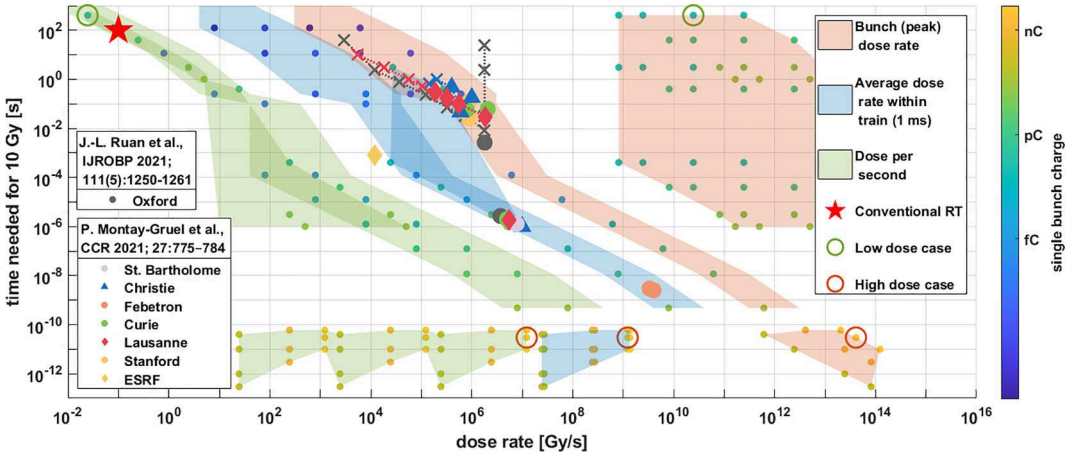

Fig. 4. The worldwide unique parameter space available at PITZ in comparison with state-of-the-art FLASH RT and conventional radiation therapy. The vertical axis shows the time needed to deliver 10 Gy and the horizontal axis shows the dose rate for 3 different estimations: The red area shows the available bunch or peak dose rates; the blue area shows the available average dose rates within the bunch trains and the green area shows the available dose rate averaged over a full second. The color of individual dots represents the bunch charge that was assumed for the individual PITZ operation parameter set (see legend on the right). The two conditions listed in Table 1 are marked with circles. The conditions to obtain reproducible FLASH effects are included as fully filled data points in the center of the plot and cases which could not prove the FLASH effect are marked with crosses as summarized by [14,37]. A star is added to represent conventional radiation therapy in the upper left corner. The PITZ parameter space available on the right side of and below the colored markers displayed in the center of the plot is yet unexplored and unexploited territory and gives potential for further improvement of FLASH RT in future. It must be noted that the colored areas show parameter combinations, which can be obtained quite easily, but none of the colored areas are sharp edged, since the parameter range can also be extended beyond the colored areas. (For interpretation of the references to color in this figure legend, the reader is referred to the web version of this article.)

biological observation characterized *in vivo*, the combination of careful selection of physical parameters and *in vivo* study are required to validate the FLASH effect [38]. It requires studying the biological effects of FLASH RT on small model organisms.

The fourth work package of the R&D program is dedicated to a beam energy upgrade of the PITZ accelerator to about 250 MeV and aims for the definition of optimum beam parameters for clinical treatment of different types of tumors. Afterwards, radiation biology, very high energy electron (VHEE) therapy, and FLASH RT experiments can be performed with thicker samples like e.g. body phantoms, biological tissue, living biological samples. Fig. 5 shows a tentative schedule of the four work packages described above.

3.1. Preparations for FLASH𝒶𝒹@PITZ: R&D beamline, dosimetry, simulations

In 2021, the installation of beamline components to conduct FLASH RT experiments at PITZ started. The FLASH RT beamline will start with a dipole switchyard, branching this part off from the straight THz beamline which was commissioned in 2022 (see 'Tunnel 2' in the schematics of Fig. 1). This has the big advantage that a lot of knowledge regarding beam transport can be reused from the THz project. That is because both beamlines work in a similar parameter space with high bunch charges and long bunch trains and diagnostics and other hardware is shared for most of the way. A first detailed design of the FLASH RT beamline will be discussed in Section 4.2 (see Fig. 9 there). The beam will be transported through an exit window to the experimental test area for the FLASH RT studies which has a dimension of at least 2 m width, 6 m length, and 3 m height.

To prepare for the radiation biology and FLASH RT experiments at PITZ, the detailed beam parameters at the treatment area will be characterized. These parameters include bunch charge, bunch length and transverse bunch size, also along the bunch trains. Besides beam dynamics simulations, which guide the way to reach the wanted beam parameters, different beam diagnostics devices will be used to measure the obtained beam parameters at the experimental area.

The new beam parameter space that is accessible at PITZ will also require a thorough characterization of the needed radiation dosimetry devices. Challenges are the shortness of the irradiation pulses down to the picosecond regime and the high particle density in the bunches (up to 3×10^{10} electrons per bunch). To address this issue, a collaboration with the PTB in Braunschweig and the UHDpulse Consortium was established [39]. This collaboration aims for providing the metrological tools needed to establish traceability in absorbed dose measurements of UHDR particle beams. Within this collaboration, dosimetry experts will contribute in the development of suitable methods and devices for the yet unexplored beam conditions. Different existing dosimetry technologies will be tested at PITZ (see Section 4.5) also beyond their current use range.

The *in silico* simulations and predictions are of high importance for quick and reliable progress in radiation biology and the corresponding research and development. Starting from the prediction and reproduction of dosimetry experiments, via the preparation and interpretation of *in vitro* and *in vivo* experiments with biological models they will also be essential for the clinical translation of FLASH𝒶𝒹@PITZ. Furthermore, we hope that with better understanding of the FLASH effect with decisive experimental data and including the primary findings in simulation models that extensive *in silico* simulations will substantially contribute to reduce animal experiments.

3.2. Studies of biological effects at FLASH𝒶𝒹@PITZ

Investigations of biological effects of FLASH radiation are realized by the work packages 2 and 3 that focus on *in vitro* and *in vivo* studies, correspondingly, and will mainly run in parallel. The *in vitro* preparatory step is dominant in the beginning, as long as *in vivo* studies of UDHR and FLASH radiation effects are not yet possible. This is in order to provide the required evidence for regulatory organization of animal studies. The PITZ beam validation for FLASH effect is planned *in vivo* "as soon as possible". The continuous combination of *in silico*, *in vitro* and *in vivo* studies will give us an opportunity to harmonize the running studies based on accumulated experimental data.

The planned biological studies will investigate the FLASH radiation effects with molecular, cellular, tissue, and whole-organism models (Fig. 6). The general experimental workflow requires exposure to the radiation, and evaluation of the follow-up changes in each model's structure and functionality. The studies will focus on simulations and experimental characterizations, both quantitatively and qualitatively. E.g. the FLASH effect will be studied for a fixed total deposited dose as a function of the individual bunch length, the bunch train length and the average dose per second. Other important experiments are to be performed to confirm that the FLASH effect can be maintained or even extended by applying scanning electron beams over a tumor volume. The downstream chemical and biological responses to FLASH radiation will be assessed in strict comparison to conventional radiation protocols (with <5 Gy/min) in order to provide toxicological assessment and a dose–response correlation to elucidate the therapeutic potential of the PITZ electron beam.

Rooms and laboratories at TH Wildau as an animal facility for husbandry, welfare and with diagnostics capabilities are planned close to PITZ. In a neighboring building to the accelerator tunnel a small welcome, storage and welfare facility will be set up for the animals before/after irradiation and transport. The animal facility at TH Wildau is planned to enable basic/common as well as high technological animal research. Following the common practice worldwide, the animal facility will support the *in vivo* evaluation of biological effects of FLASH radiation to realize an important step of preclinical therapy development.

3.3. PITZ energy upgrade

Currently the beam energy at PITZ is limited to about 22 MeV, which limits the reach of electrons in water to a few centimeters. This is

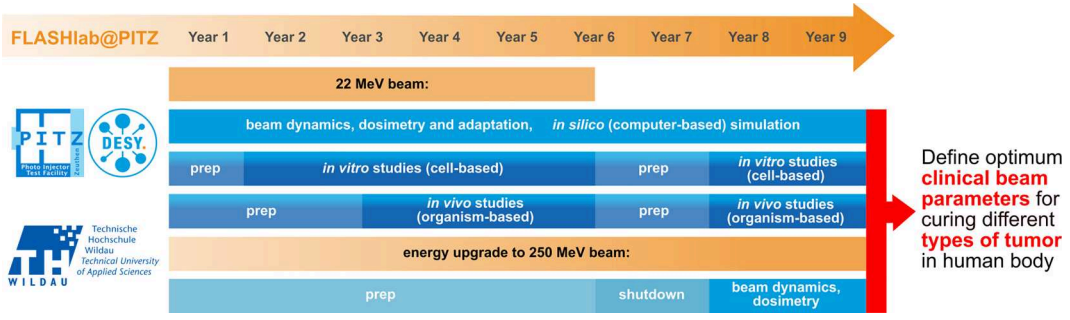

Fig. 5. Schematic time structure of the four work packages of the presented project. © 2022 Frank Stephan.

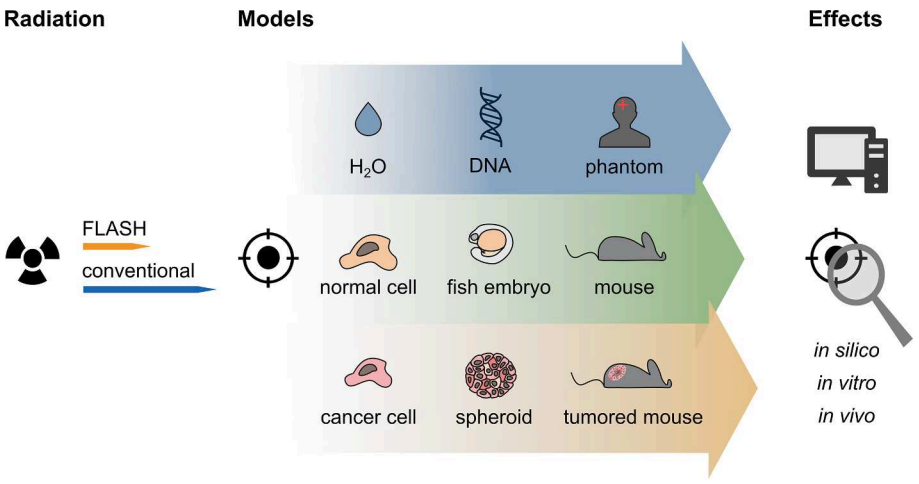

Fig. 6. Overview of the planned studies on chemical and biological effects of FLASH radiation at FLASH𝒻𝒶𝓈𝒽@PITZ: The effects of FLASH radiation should be modelled and evaluated in comparison with the radiation delivered at conventional dose rate. Target models to be studied include molecules, phantoms, cells, tissues and whole organisms. The decisive evaluation of the FLASH effect has to be done with *in vivo* models as soon as possible. In silico simulations are integrated into the project to simulate and predict physical, chemical, and biological effects of the FLASH beam and predict treatment responses. Biological effects of radiation are to be evaluated *in vitro* and *in vivo* on the structure and functionality of the studied biological models. © 2022 Frank Stephan.

sufficient to study radiation biology and FLASH RT for small subjects like mice or close to the surface for thicker samples, e.g. skin cancer. But cancer cells inside of larger patients like humans cannot be treated. Therefore, an energy upgrade to enable VHEE radiotherapy [28,40] is the next logical step. Another advantage of the beam energy upgrade, which is at least as important, is that with high beam energy the radiation distribution in the volume can be much better controlled. This means that one would.

1. have a well-defined and homogeneous dose delivery over the entire tumor tissue, especially when the tumor is in a depth from the surface of more than 2–3 cm
2. have a smaller and constant irradiation beam size over the entire sample depth, and
3. perform pencil beam scanning, especially for treating tumors beyond 1–2 cm from the surface (see last paragraph of Section 2.3).

To illustrate the benefit of increased beam energy, Fig. 7 shows the energy deposition for the two cases of 22 and 250 MeV beam energy and three different beam sizes. It is clear that the lower energy electron beam undergoes significant multiple scattering, which widens the beam distribution quite quickly, and also the total reach (depth) is quite limited. On the other hand, the high energy electron beam mainly keeps its size and allows a much more homogeneous dose delivery over the entire irradiation volume. By extending the water volume in the beam direction, it was shown that the treatment range can be extended by a factor 5 with respect to the 22 MeV case, so that up to 30 cm in depth could be handled, a depth sufficient for treating humans.

The beam energy upgrade at PITZ is planned to be realized by using a super-conducting cryomodule with eight super-conducting European-XFEL-like cavities. They together should provide an energy gain of about 240 MeV with an RF pulse length such that 1 ms long bunch trains with up to 5 nC charge per bunch can be accelerated. This option maintains the full flexibility in the choice of the beam parameters, which PITZ can produce. This is essential for optimizing the beam parameters to maximize the therapeutic window for different kinds of tumors in a human body.

4. Preparations for realization

4.1. X-ray fluorescence imaging (XFI) as novel method for image-guiding in FLASH therapy

Due to the high flexibility and unique pulse train structure at PITZ, XFI based image guiding together with FLASH RT could potentially be combined so that diagnostics and treatment could be realized within 1 ms. Due to the high relevance of this approach to further reduce the irradiation of healthy tissue, the preparatory studies for this concept are already started in an early stage of the project realization.

XFI allows the detection and tracking of medical agents such as drug compounds, nanoparticles for drug delivery, immune or tumor cells, as well as other entities, if those are labelled with markers which emit fluorescence photons upon excitation with a pencil beam, e.g., brilliant X-rays from a synchrotron. As the spatial resolution of the modality

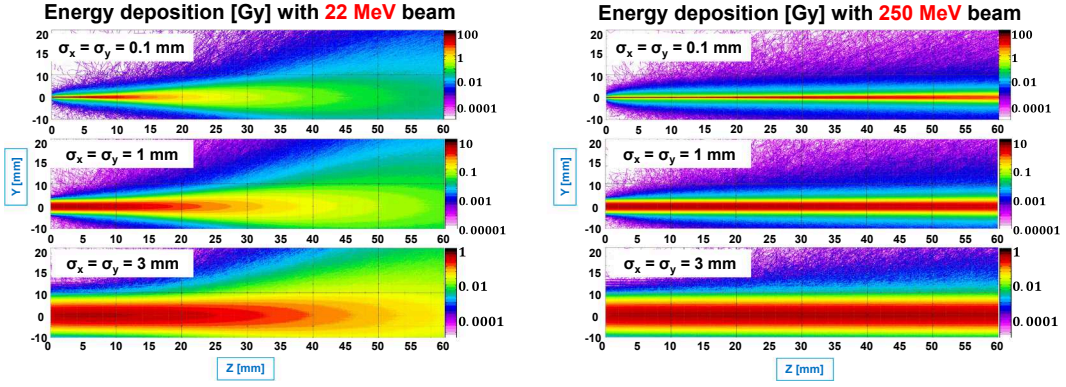

Fig. 7. Energy deposition in Gray for 1 bunch with a charge of 100 pC and a beam energy of 22 MeV (left) and 250 MeV (right) for 3 different beam sizes in water. The simulation shows the energy deposition when integrating over a water slice thickness of 1 mm. The initial transverse beam distribution was assumed to be Gaussian and the sigma of the distribution was chosen for the 3 cases: 0.1 mm (upper line), 1 mm (middle line) and 3 mm (lower line). The simulations are shown for the first 6 cm of the water volume. © 2022 Frank Stephan.

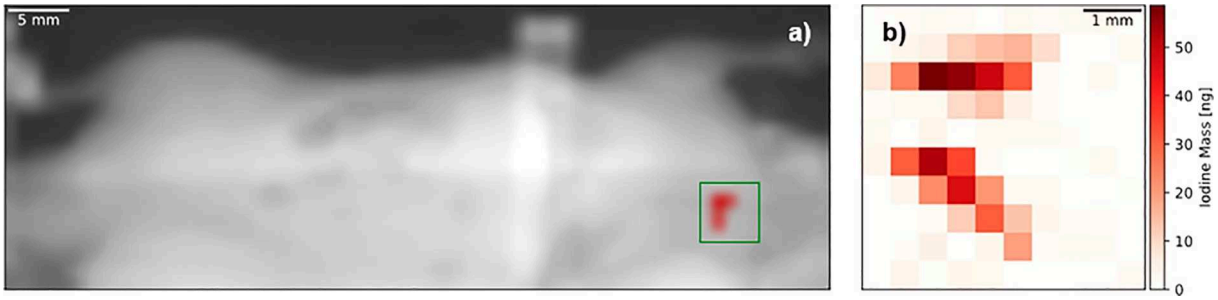

Fig. 8. X-ray fluorescence imaging full-body (a) and fine scan of the thyroid region (b) of a mouse. The left map depicts the number of Compton-scattered photons for each scan position. As seen, the only visible iodine concentration is the natural one found in the thyroid with the local iodine mass in the beam volume as retrieved from data analysis (each pixel of the fine scan covers an area of 0.25 mm^2 and shows the amount of iodine K_α fluorescence photons) [41].

solely depends on the applied beam diameter, structures smaller than 1 mm can be detected, as demonstrated in [41,42] and shown in Fig. 8, where the endogenous iodine content of a murine thyroid was determined with a spatial resolution of only 0.25 mm^2. In this case, no additional marker was needed since iodine already is an XFI-visible element which can also be used as marker for entities of interest.

Besides the substantially higher detection sensitivity than X-ray absorption imaging, XFI has the additional advantage that it can be applied over arbitrarily long time windows as the used markers do not decay over time like radiotracers used in PET or SPECT imaging. Furthermore, XFI offers multi-tracking, i.e., the simultaneous tracking of different entities like for example various types of immune cells which contribute to immune-mediated diseases. Moreover, the high sensitivity of XFI allows the detection of very low numbers of quantities, e.g., only a few hundred tumor cells labelled with functionalized nanoparticles, as demonstrated in [43].

So far, X-rays are used for the excitation of the fluorescence photons [41–46], however, also low intensity electron beams can be applied as incident radiation. This use of electron beams allows an online localization of a labelled tumor, e.g., with functionalized gold nanoparticles, before the immediate treatment of tumorous tissue with a high intensity electron beam. It has been shown in [44] that functionalized gold nanoparticles specifically bind to dedicated target regions and that XFI is capable of localizing them, thus, offering the potential to combine diagnostics and therapy.

With the setup described in Section 2, the first part of a bunch train with low charge can be used to excite fluorescence in the targeted tumor to allow precise localization, as given by the applied scanning pencil beam diameter. A subsequent second part of the bunch train with much higher charge can then be used to apply ultra-high dose rate, short treatment time (FLASH RT). The whole procedure, e.g., the exact tumor localization as well as its treatment, can hence be done within 1 ms, a time scale at which organ motion such as breathing does not play a role any more. Moreover, this exact localization allows the restriction of the treatment volume to the tumorous tissue only, while surrounding healthy tissue is spared.

4.2. Beamline design

To fully employ the 22 MeV beam for studying FLASH RT, a dedicated beamline has been designed in order to send electron beams with varying bunch charge and length to the experimental station. The new beamline will be installed in PITZ tunnel 2 (see upper part of Fig. 1). This part of the PITZ beamline is shown in more detail in Fig. 9: the FLASH*al*@PITZ beamline will be in parallel to the THz FEL beamline, first translated by a dogleg, then captured and focused down to the exit window (see Section 4.4) by two quadrupole triplets. A transverse deflecting system (TDS) could be used to measure the longitudinal bunch profile; the sweeper will kick the beam transversely for tumor painting studies; a short solenoid after the exit window is under consideration for imaging the electron beam to the sample.

The dogleg consists of two dipole magnets which deflect the beam horizontally in opposite directions and two pair of quadrupole magnets. By properly tuning the strengths of the quadrupoles the dogleg is made achromatic (i.e. vanishing horizontal dispersion functions: $\eta_x = 0, \eta_{x'} = 0$), thus preserving the quality of the beam from the photoinjector. The transfer matrix of the dogleg has a nonzero longitudinal dispersion R_{56} (0.11 m here), allowing to manipulate the bunch length by tuning the longitudinal phase space with the booster accelerator phase. A pair of sextupole magnets is also being considered to minimize higher order effects. Following the dogleg is a quadrupole triplet that captures the electron beam before it is focused with another quadrupole triplet down

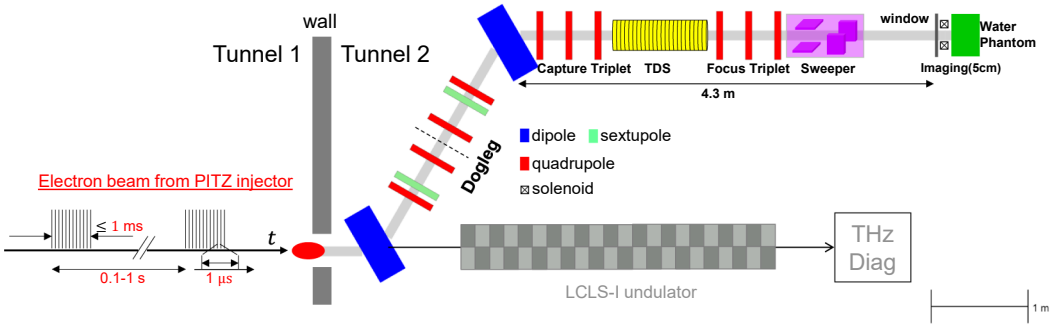

Fig. 9. The layout of the FLASH*al*@PITZ beamline. The FLASH*al*@PITZ beamline (upper beamline) will be in parallel to the THz FEL beamline (lower beamline), translated there by a dogleg, which consists of dipole magnets for bending, quadrupole magnets for focusing and possibly sextupole magnets to minimize higher order effects. The following 4.3 m long beamline contains a transverse deflecting system (TDS) to measure longitudinal bunch profiles, and a sweeper for transverse beam kicking; the beam is captured from the dogleg and focused down to the exit window by two quadrupole triplets. Subsequently the experimental area for the R&D on FLASH RT is located.

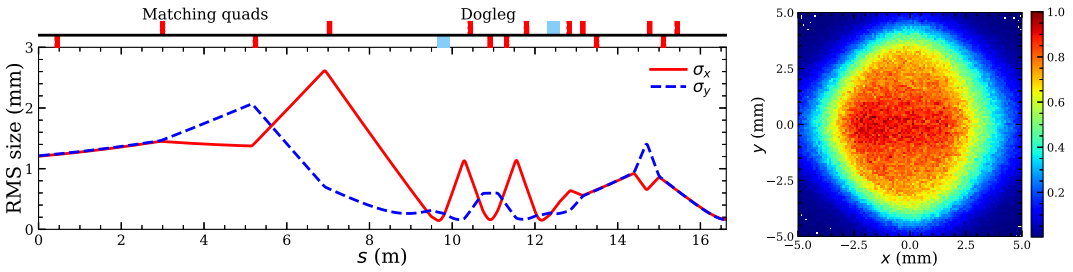

Fig. 10. Transport of a 1 nC bunch along the FLASH*al*@PITZ beamline. The left side of the figure shows the development of the beam size along the PITZ beamline for a tightly focused beam at the exit window. The right side shows the beam profile for a different beam transport with a larger spot size at a location 2 cm downstream of the exit window. © 2022 Frank Stephan.

to the exit window, while optionally being kicked transversely by the sweeper (see Section 4.3).

Start-to-end simulations from the photocathode to the exit window have been performed with typical bunch charges. Fig. 10 shows the results for a 1 nC bunch charge. Four upstream quadrupoles in the existing PITZ beamline were optimized to match the electron beam into the dogleg, then the FLASH*al*@PITZ beamline successfully delivers the beam to the exit window. In Fig. 10 (left side) one sees that a small beam (~0.2 mm rms transverse size) can be generated and transported, e.g. to do pencil beam scanning. By choosing different transport parameters, larger spot sizes can be generated to irradiate the full tumor in one shot. Fig. 10 (right side) shows an example with a ~2.4 mm rms transverse size 2 cm downstream of the exit window which could correspond to the sample position. The simulations were performed with the software suites ASTRA [47], Ocelot [48] and Geant4 [49].

The scattering effects in the exit window can cause significant transverse divergence of the 22 MeV electron beam, making its size blow up during the drift in air. In order to minimize this effect, an imaging system with magnets and a total length of 5 cm (as shown in Fig. 9) is being investigated to image the focused beam at the window to the surface of the irradiated samples. Another option to minimize the window scattering effect will be putting the samples as close as possible to the window. Both options are under further studies.

4.3. Bunch distribution with fast kicker systems

To irradiate extended samples with ultra-high dose rates, a system of fast deflector ("kicker" – also called "sweeper") magnets will be employed. The requirements on the system are the distribution of up to 4500 bunches in a train of 1 ms duration, which already includes the photo cathode laser system update in 2023. The transverse distribution of the pencil beams will be flexible over a maximum area of currently 625 mm^2 (see also Fig. 11, top right). Especially the flexible variation of the deflection strength between bunches in multiple steps at a bunch separation of <1 µs is challenging and we are not aware of an existing system which fulfills these requirements. Therefore, the kicker system will be implemented in three steps, following the progress of the necessary research and development of the final system.

4.3.1. Conventional, one-dimensional distribution of flat beams

At first instance, an available, inductive kicker magnet design [50] with the corresponding driving electronics will be implemented. The magnet consists of a flat copper conductor laid in a single loop around a ceramics chamber. Pulsed currents are provided by a power amplifier, which allows to amplify arbitrary input current signals to a maximum of ± 100 A on a time scale of 10 µs. Hence, time gaps in the electron bunch trains have to be foreseen in case the next current level cannot be reached stably within one nominal bunch separation time. A sketch of this system with an exemplary input current is shown in Fig. 11 (current curve in lower right corner). In this first phase, only one kicker will be installed to distribute bunches in one direction. Bunches will be defocused in the static plane to irradiate samples which extend in both transverse planes.

4.3.2. Fast bunch distribution

To allow for distribution of bunches at up to 4.5 MHz bunch repetition rate, a new kicker system is being developed. Kicker systems with even shorter bunch-to-bunch separations are being developed already at DESY [51], whereas the challenge will be to provide a fully flexible pulse amplitude and polarity on such short timescales. A collaboration with the Institute for Pulsed Power and Microwave Technology (IHM) of the Karlsruhe Institute of Technology (KIT) has been established for this development.

A first prototype will be added to the inductive kicker system

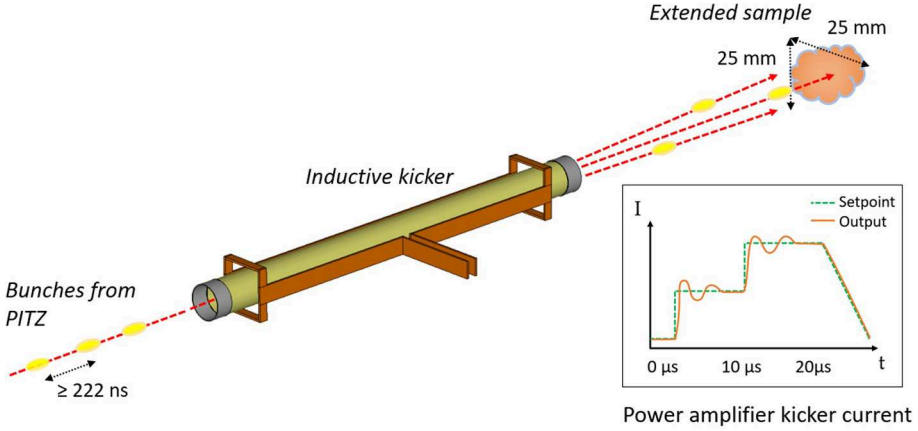

Fig. 11. Sketch of FLASH*al*@PITZ initial bunch distribution system. Inset graph shows an exemplary current waveform of the driver electronics of the kicker magnet. © 2022 Gregor Loisch.

described above to enable distribution of a bunch train of at least 25 bunches in both transverse planes with some constraints on e.g. minimum bunch separation.

4.3.3. *Fully flexible distribution of high energy, long bunch trains*

In its final implementation, the beam distribution system will consist of two of the fast bunch deflector systems described above, capable of flexibly distributing the full train of 4500 bunches at a beam energy of up to 250 MeV over a sample area of 25 mm by 25 mm (see also Fig. 11).

4.4. *Considerations on an exit window*

The electrons used for irradiating biological samples must leave the beam line vacuum through an exit window. Although having to withstand static atmosphere pressure, its thickness should be small in terms of radiation length to minimize scattering. On the other hand, the window must withstand the short thermomechanical impact as a consequence of the related energy loss of the incoming bunch trains. This is most severe for tightly focused, long bunch trains of high charge electron bunches.

Thus, the window has to fulfil the following criteria, sorted according to their relevance:

1. Scattering effect as small as possible.
2. Allowed beam spot size due to pulsed load by one bunch train as small as possible.
3. Tolerable average load by repeating bunch trains as large as possible (calculation of quasi-equilibrium temperature).

The goal is to identify the optimal window for the specific needs of our application.

Table 2

Comparison of window materials. The summarized results are based on simplified analytical formulae. The scattering angle is derived by the Moliere approximation [52]. In pulsed beam applications, every passage of a bunch train causes a sudden temperature rise ΔT_{inst}, which creates mechanical stress. A simple model [53] transfers the endurance limit of the material into the allowed tolerable instantaneous temperature jump tol(ΔT_{inst}). From this the minimum allowed Gaussian beam spot size σ_{min} is gained by the materials stopping power and its specific heat capacity. The quasi equilibrium temperature rise ΔT_{eq} around which the temperature jumps oscillate, assumes a non-pulsed beam of the same average current as the pulsed one has. Only radial heat conduction between the axis of the Gaussian heat source and a heat sink at the outer radius is considered.

Parameter	Unit	CFC	Kapton®	Be	Al	Ti
Stopping power $\left(\frac{1}{\rho}\frac{dE}{dz}\right)_{ion}$ [54]	$\left[\frac{\mathrm{MeV}\cdot\mathrm{cm}^2}{\mathrm{g}}\right]$	1.82	1.7 [2)]	1.63	1.71	1.59
Material density ρ	$[\mathrm{g/cm^3}]$	1.6	1.42	1.85	2.7	4.54
Tensile strength $\sigma_{0.2}$	[MPa]	130	120	300	110	350
Endurance limit σ_{cycl}	[MPa]	110	70	240	40	200
Minimal window thickness t_1 to withstand 1 bar pressure difference	[mm]	0.41	0.43 [*)]	0.27 [*)]	0.44 [*)]	0.25 [*)]
Window thickness t_2 as for envisaged window	[mm]	0.51				0.05
Calculated scattering angle $\theta_M(22\mathrm{MeV})$	[mrad]	**t_2: 21**	**t_1: 18** [*)]	**t_1: 12** [*)]	**t_1: 35** [*)]	**t_2: 17**
Tolerable instantaneous temperature jump tol(ΔT_{inst}) / tolerable energy density tol$\left(\frac{\Delta Q}{\Delta m}\right)$	[K] / $\left[\frac{\mathrm{J}}{\mathrm{g}}\right]$	**480** [1)] / 340	**180** / 200	**79** / 70	**15** / 14	**140** / 79
Minimal allowed beam spot size $\sigma_{min}(5\mu\mathrm{C})$	[mm]	**0.7**	**0.8**	**1.4**	**3.1**	**1.3**
Thermal diffusion length $\Lambda(1\mathrm{ms})$	[mm]	0.16	0.1	0.3	0.28	0.083
Quasi equilibrium temperature drop $\Delta T_{eq}(\sigma_{min}, 5\mu\mathrm{C}, 10\mathrm{Hz})$	[K]	**220**	**330**	**31**	**25**	**760**

[1)] 70% of estimation since C is brittle, [2)] assumed, no data available

[*)] overestimated thickness due to simplified calculation

4.4.1. Material comparison

In order to motivate the selection of the intended window type, a rough comparison of materials, which are commonly used in this type of application, was conducted. We take metals (Be, Al and Ti), a polyimide plastic like Kapton® and a very advanced composite, namely carbon fiber reinforced carbon (CFC – one side coated with pyrolytic graphite for leak-tightness). Table 2 shows the results for a ∅ = 34 mm window and 1 ms trains, repeating with 10 Hz and containing 5000 bunches of 1 nC each. They are scalable with the applied beam parameters.

Referring to the above criteria, material ranking is indicated by coloring the corresponding rows from green (well suited) to red (bad choice). Although Be is a wonderful candidate in every respect, it will be out of discussion due its hazard properties. In terms of minimum scattering and pulsed beam capability Ti, Kapton and CFC are top of the list. While the 50 μm thin Ti-sheet creates less scattering, the CFC has better cyclic strength capability and thus allows smaller beam spots. Kapton behaves in between of both. Al has a low endurance limit and the allowed beam spot must be large to avoid a window failure. In high repeating pulse mode, when the energy deposition of subsequent bunch trains adds significantly, thermal conduction is decisive for the ranking. That is why the CFC type is clearly the best choice if all three criteria are of relevance.

FLASH*forward*@PITZ uses single bunch trains with a very low repetition. Thus, only the first two criteria are of importance and Ti is a good window material. A 50 μm thick Ti-foil assembled in a commercially available DN40 flange set is already in use in another facility at DESY and therefore intended to be used here as well. Kapton can serve as a future option.

For PITZ like beams with 10 Hz repetition rate, the CFC window is of course very attractive in all aspects, but challenging in production. A full metal version with brazing technology was not successful. But a leak tight solution exists, where the CFC disc is glued into the surrounding vacuum pipe. Beam tests with this window are planned at PITZ to determine its limits, especially tol($\Delta Q/\Delta m$) experimentally. If the results are still promising like in Table 2, other radiation hard assemblies than brazing might be investigated. The glued version suffers from limited lifetime due to radiation damage of the epoxy compound, which is expected after passage of about $3{\cdot}10^7$ bunch trains with 5000 nC each. At 10 Hz this corresponds to a continuous operation time of about 800 h.

The energy upgrade to 250 MeV will not affect the selection of window material, since the thermomechanical impact for thin materials does not depend on the beam energy in this range, while the scattering is reduced by an order of magnitude.

4.4.2. Monte Carlo simulation results

To support the analytical results the FLUKA Monte Carlo code [55,56] was used to calculate the energy deposition map in the exit window and the electron beam parameters behind it for two windows which will be used for first experiments at PITZ: the first is a 50 μm thick titanium window, the second one is based on graphite. It consists of a 500 μm CFC carrier material (1.5 g/cm^3), that is coated on one side with a 10 μm thick layer of pyrolytic graphite (PyC, 2 g/cm^3). A Gaussian fit on the scattering profile of 22 MeV electrons exiting these windows delivers a rms value of 17.3 mrad (titanium window) and 19.6 mrad (graphite window) and agrees fairly well with calculated results which are shown in Table 1.

The interaction of an electron bunch with the window generates energy losses, which transform into a thermal energy load on the window. Fig. 12 shows the heat density as deposited by a single 1 nC bunch in a titanium or graphite window as a function of the radial distance from the beam center. According to beam dynamics simulations (see Section 4.2) a round bunch with a minimum beam size of σ = 0.2 mm can be expected at the window. Such a bunch induces a heat density profile in the window with a peak value of $q_{max} = 2.41$ J/cm^3 (0.53 J/g) for titanium and $q_{max} = 0.91$ J/cm^3 (0.61 J/g) for graphite. Calculations give 0.64 J/g for titanium and 0.73 J/g for the graphite window.

4.5. Dosimetry

4.5.1. Monte Carlo simulation results

A Monte Carlo study of scenarios expected for FLASH*forward*@PITZ experiments was performed using the Geant4 toolkit [49] with a PITZ-like mono-energetic electron beam of 22 MeV. The depth doses within a water phantom were simulated for a range of beam sizes as shown in Fig. 13.

The electron beam dose distribution inside the phantom decreases exponentially behind an initial dose peak at a depth Z_{max} below 10 mm (Fig. 13 left). The parameter Z_{max} and thereby the beam penetration can be tuned slightly by adjusting beam size and energy. Another important parameter used to estimate the beam penetration is the R_{50} depth corresponding to 50 % of the maximal dose in the depth dose curve (Fig. 13 right). R_{50} is linearly depending on the beam size with values between 10 mm and 30 mm for the simulated range.

4.5.2. Detector needs

In the subsequent experiments the dose distributions need to be characterized. With an average dose rate of up to ~ 10^7 Gy/s and peak dose rates per bunch of up to ~10^{14} Gy/s (Fig. 4) the dosimetry is a major challenge. There is no detector yet known that provides reliable measurements and linearity up to such high dose rates. So far only the passive detectors alanine and radiochromic films have been tested up to a limit of 10^{10} Gy/s. Other common detectors for dosimetry are ionization chambers, silicon and diamond solid-state detectors, and plastic scintillators [57–59].

Each detection method has different limits at which saturation occurs. Ionization chambers can only be used up to a few hundred Gy/s

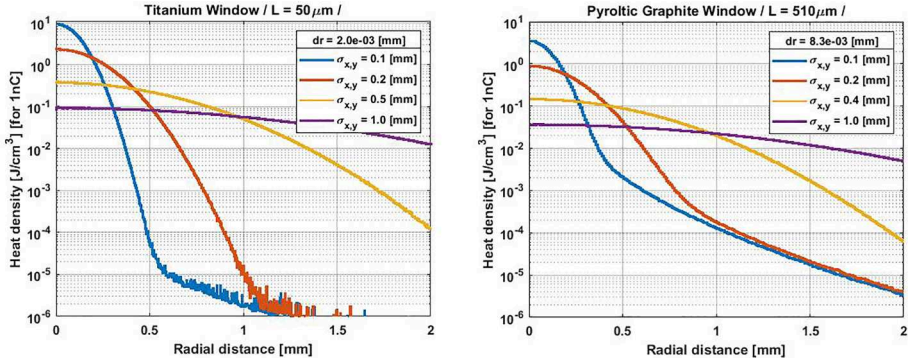

Fig. 12. The deposited heat density by a single 1 nC bunch in the 50 μm thick titanium (left) and the 510 μm thick graphite (right) window for different beam spot sizes, as a function of the radial distance from the beam center. The curves correspond to a beam spot size σ of 0.1 mm, 0.2 mm, 0.5 mm and 1 mm. For a bunch with σ = 0.2 mm the maximum temperature rise of $\Delta T = q_{\max}/(\rho c)$ on the axis is 0.96 K for titanium and 0.85 K for graphite.

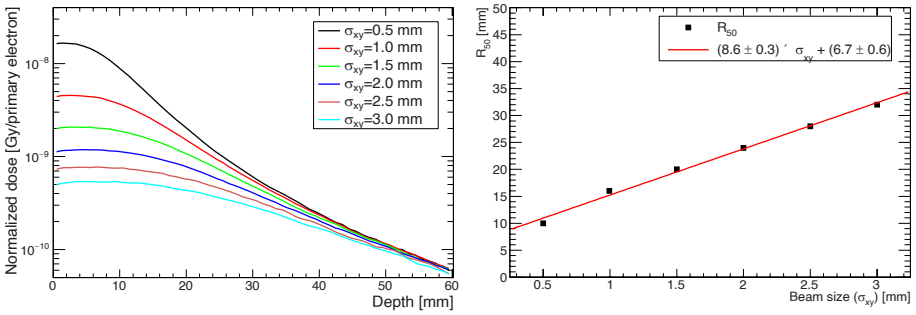

Fig. 13. Calculation of the dosimetric properties of a 22 MeV mono-energetic electron beam: Depth dose curves at the beam axis for different Gaussian beam sizes σ_{xy} at the surface of a water phantom with dimensions $61 \times 61 \times 60\,mm^3$ (left); R_{50} variation in terms of the beam size σ_{xy} (right). © 2022 Frank Stephan.

[60,61]. The parallel plate ionization chamber PPC05 from IBA Dosimetry [60] will be used at PITZ for calibration and as a reference for other detectors. Gafchromic EBT-XD films [62] are chemical dosimeters and their linearity at the ultra-high dose rates available at PITZ will be investigated. Alanine is planned to be used for cross dosimetry. Other potential candidates for investigation could be pyroelectric and graphite calorimeters [63–65], modified ionization chambers, Cherenkov detectors, fluorescence detectors and magnetic inductive coils [66–68].

Efforts are underway to make ionization chambers and other commercially available detectors work at FLASH dose rates. For FLASH*forward*@PITZ, radiation hardness is a major challenge. Although the total dose of a treatment will not exceed 100 Gy, the facility and the dosimetry detectors may be exposed to a much higher dose, even in the order of MGy. Furthermore, a very high readout speed is one way to cope with the high dose rates and prevent the detector from saturating. Detectors from particle physics experiments such as silicon pixel sensors are especially designed for both, radiation hardness and high readout speed. Therefore, they seem to be potential candidates to be tested at PITZ.

Different kinds of silicon particle physics detectors will be tested, all of them with a different sort of optimization: The MALTA sensor [69] combines fast readout and a very high radiation hardness with an adjustable readout threshold, which could solve the problem of saturation at high dose rates. The DECAL sensor [70] is more specialized for calorimetry and may be better suited for dosimetry. The Timepix sensor which is a hybrid pixel detector for particle tracking [71] has a focus on an even higher timing precision. It is planned to do measurements with a customized Timepix3 in cooperation with the company Advacam [72].

The requirements for time resolution are high: at PITZ a bunch with maximum charge (5 nC) is approx. 30 ps long. In this time a detector (1 cm^2, 3 cm in water) will be hit by an avalanche of up to $5.5*10^{10}$ primary and secondary particles. The time resolution required to resolve individual bunches at PITZ will push even these detectors from particle physics to their limits. Fortunately, the future development in particle physics is focused on even better time resolution. Low Gain Avalanche Detectors (LGADs) are being developed to achieve a time resolution of 10–30 ps [73–75]. These sensors are being incorporated in test beams at DESY, and are a possible upgrade path for PITZ.

5. Summary

Here we described the FLASH*forward*@PITZ platform, which is planned to be realized at the PITZ facility over the next several years. The extremely wide parameter range accessible at PITZ together with its full flexibility and tight beam control capabilities will give worldwide unique opportunities to push forward the understanding, optimization and application of FLASH RT. To summarize the unique capabilities of the electron bunches and their time structure, PITZ will allow a new approach to FLASH RT with

- an individual bunch charge tunable over more than 5 orders of magnitude to the wanted local radiation dose and dose rate,
- a bunch length adjustable over about a factor 10 for fixed bunch charge to tune the wanted instantaneous dose rate for fixed dose per bunch,
- a beam size adjustable to match the tumor size or for scanning the tumor area with pencil beams allowing local dose variation,
- a bunch repetition rate and bunch train length tunable over 3 orders of magnitude to adjust the local dose and the average dose rate,
- a bunch train repetition rate adjustable between 1 and 10 Hz to tune the local dose and the average dose rate by another factor 10.

Besides simulations also experimental activities have already started as preparation of the upcoming experiments. A radiation biology beamline is in the process of being added to the PITZ accelerator, including an optimized electron beam transport, a beam exit window, specialized radiation detection and novel diagnostic techniques.

The final goal of FLASH*forward*@PITZ is to define the optimum beam parameters and treatment modalities in order to maximize the therapeutic window for the safe treatment of different kinds of tumors, in their specific surroundings and at human scale. This means that new cancer radiation therapy treatment modalities are developed which mitigate the risk of harmful side effects and allow cancer treatment strategies with higher efficacy and efficiency.

Declaration of Competing Interest

The authors declare that they have no known competing financial interests or personal relationships that could have appeared to influence the work reported in this paper.

Acknowledgements

This research did not receive any specific grant from funding agencies in the public, commercial, or not-for-profit sectors. Nevertheless, the work very strongly profited from the continuous support of DESY and the TH Wildau, as well as from the synergies with the high brightness electron source development for the free electron laser user facilities FLASH, the XUV and soft X-ray Free-Electron Laser Facility at DESY, and the European XFEL, as well as from the preparations for a proof-of-principle experiment for a THz SASE FEL at PITZ.

References

[1] Galeaz C, Totis C, Bisio A. Radiation resistance: A matter of transcription factors. Front Oncol 2021;11:662840. https://doi.org/10.3389/fonc.2021.662840.
[2] Schaue D, McBride WH. Opportunities and challenges of radiotherapy for treating cancer. Nat Rev Clin Oncol 2015;12:527–40. https://doi.org/10.1038/nrclinonc.2015.120.
[3] Mohan G, T P AH, A J J, K M SD, Narayanasamy A, Vellingiri B. Recent advances in radiotherapy and its associated side effects in cancer - A review. JoBAZ 2019;80:14. https://doi.org/10.1186/s41936-019-0083-5.

[4] Trifiletti DM, Zaorsky NG. Absolute Clinical Radiation Oncology Review. Springer Nature Switzerland AG; 2019.
[5] Hornsey S, Alper T. Unexpected dose-rate effect in the killing of mice by radiation. Nature 1966;210:212–3. https://doi.org/10.1016/j.radonc.2003.03.001.
[6] Town CD. Effect of high dose rates on survival of mammalian cells. Nature 1967; 215:847–8. https://doi.org/10.1038/215847a0.
[7] Berry RJ, Hall EJ, Forster DW, Storr TH, Goodman MJ. Survival of mammalian cells exposed to x rays at ultra-high dose-rates. Br J Radiol 1969;42:102–7. https://doi.org/10.1259/0007-1285-42-494-102.
[8] Favaudon V, Caplier L, Monceau V, Pouzoulet F, Sayarath M, Fouillade C, et al. Ultrahigh dose-rate FLASH irradiation increases the differential response between normal and tumor tissue in mice. Sci Transl Med 2014;6:245ra93. https://doi.org/10.1126/scitranslmed.3008973.
[9] Montay-Gruel P, Petersson K, Jaccard M, Boivin G, Germond J-F, Petit B, et al. Irradiation in a flash: Unique sparing of memory in mice after whole brain irradiation with dose rates above 100Gy/s. Radiother Oncol 2017;124:365–9. https://doi.org/10.1016/j.radonc.2017.05.003.
[10] Montay-Gruel P, Acharya MM, Petersson K, Alikhani L, Yakkala C, Allen BD, et al. Long-term neurocognitive benefits of FLASH radiotherapy driven by reduced reactive oxygen species. PNAS 2019;116:10943–51. https://doi.org/10.1073/pnas.1901777116.
[11] Simmons DA, Lartey FM, Schüler E, Rafat M, King G, Kim A, et al. Reduced cognitive deficits after FLASH irradiation of whole mouse brain are associated with less hippocampal dendritic spine loss and neuroinflammation. Radiother Oncol 2019;139:4–10. https://doi.org/10.1016/j.radonc.2019.06.006.
[12] Montay-Gruel P, Markarian M, Allen BD, Baddour JD, Giedzinski E, Goncalves Jorge P, et al. Ultra-high-dose-rate FLASH irradiation limits reactive gliosis in the brain. Radiat Res 2020;194:636–45. https://doi.org/10.1667/rade-20-00067.1.
[13] Alaghband Y, Cheeks SN, Allen BD, Montay-Gruel P, Doan NL, Petit B, et al. Neuroprotection of radiosensitive juvenile mice by ultra-high dose rate FLASH irradiation. Cancers (Basel) 2020;12:1671. https://doi.org/10.3390/cancers12061671.
[14] Montay-Gruel P, Acharya MM, Jorge PG, Petit B, Petridis IG, Fuchs P, et al. Hypofractionated FLASH-RT as an effective treatment against glioblastoma that reduces neurocognitive side effects in mice. Clin Cancer Res 2021;27:775–84. https://doi.org/10.1158/1078-0432.CCR-20-0894.
[15] Allen BD, Acharya MM, Montay-Gruel P, Jorge PG, Bailat C, Petit B, et al. Maintenance of tight junction integrity in the absence of vascular dilation in the brain of mice exposed to ultra-high-dose-rate FLASH irradiation. Radiat Res 2020; 194:625–35. https://doi.org/10.1667/RADE-20-00060.1.
[16] Soto LA, Casey KM, Wang J, Blaney A, Manjappa R, Breitkreutz D, et al. FLASH irradiation results in reduced severe skin toxicity compared to conventional-dose-rate irradiation. Radiat Res 2020;194:618–24. https://doi.org/10.1667/rade-20-00090.
[17] Pawelke J, Brand M, Hans S, Hideghéty K, Karsch L, Lessmann E, et al. Electron dose rate and oxygen depletion protect zebrafish embryos from radiation damage. Radiother Oncol 2021;158:7–12. https://doi.org/10.1016/j.radonc.2021.02.003.
[18] Kacem H, Almeida A, Cherbuin N, Vozenin M-C. Understanding the FLASH effect to unravel the potential of ultra-high dose rate irradiation. Int J Radiat Biol 2022;98: 506–16. https://doi.org/10.1080/09553002.2021.2004328.
[19] Fouillade C, Curras-Alonso S, Giuranno L, Quelennec E, Heinrich S, Bonnet-Boissinot S, et al. FLASH irradiation spares lung progenitor cells and limits the incidence of radio-induced senescence. Clin Cancer Res 2020;26:1497–506. https://doi.org/10.1158/1078-0432.CCR-19-1440.
[20] Velalopoulou A, Karagounis IV, Cramer GM, Kim MM, Skoufos G, Goia D, et al. FLASH proton radiotherapy spares normal epithelial and mesenchymal tissues while preserving sarcoma response. Cancer Res 2021;81:4808–21. https://doi.org/10.1158/0008-5472.CAN-21-1500.
[21] Wilson JD, Hammond EM, Higgins GS, Petersson K. Ultra-high dose rate (FLASH) radiotherapy: Silver bullet or Fool's gold? Front Oncol 2020;9:1563. https://doi.org/10.3389/fonc.2019.01563.
[22] Zhou G. Mechanisms underlying FLASH radiotherapy, a novel way to enlarge the differential responses to ionizing radiation between normal and tumor tissues. Radiat Med Protect 2020;1:35–40. https://doi.org/10.1016/j.radmp.2020.02.002.
[23] Schüler E, Acharya M, Montay-Gruel P, Loo Jr BW, Vozenin M-C, Maxim PG. Ultra-high dose rate electron beams and the FLASH effect: From preclinical evidence to a new radiotherapy paradigm. Med Phys 2022;49:1–14. https://doi.org/10.1002/mp.15442.
[24] Friedl AA, Prise KM, Butterworth KT, Montay-Gruel P, Favaudon V. Radiobiology of the FLASH effect. Med Phys 2022;49:1993–2013. https://doi.org/10.1002/mp.15184.
[25] Jolly S, Owen H, Schippers M, Welsch C. Technical challenges for FLASH proton therapy. Physica Med 2020;78:71–82. https://doi.org/10.1016/j.ejmp.2020.08.005.
[26] Corsini R, Farabolini W, Malyzhenkov A, Dyks LA, Korysko P, Sjobak KN, et al. Status of the CLEAR User Facility at CERN and its Experiments. LINAC 2022: Proceedings of the 31st International Linear Accelerator Conference; 2022 August 28-September 2; Liverpoool, UK, THPOPA05, Pre-Press Status 02-September 2022.
[27] Small KL, Henthorn NT, Angal-Kalinin D, Chadwick AL, Santina E, Aitkenhead A, et al. Evaluating very high energy electron RBE from nanodosimetric pBR322 plasmid DNA damage. Sci Rep 2021;11:3341. https://doi.org/10.1038/s41598-021-82772-6.
[28] Kokurewicz K, Brunetti E, Curcio A, Gamba D, Garolfi L, Gilardi A, et al. An experimental study of focused very high energy electron beams for radiotherapy. Commun Phys 2021;4:33. https://doi.org/10.1038/s42005-021-00536-0.
[29] Radiation Source at the ELBE Center for High-Power Radiation Sources, https://www.hzdr.de/db/Cms?pNid=971, 2017 [accessed 9 September 2022].
[30] Andruszkow J, Aune B, Ayvazyan V, Baboi N, Bakker R, Balakin V, et al. First observation of self-amplified spontaneous emission in a free-electron laser at 109 nm wavelength. Phys Rev Lett 2000;85:3825–9. https://doi.org/10.1103/PhysRevLett.85.3825.
[31] Ackermann W, Asova G, Ayvazyan V, Azima A, Baboi N, Bähr J, et al. Operation of a free-electron laser from the extreme ultraviolet to the water window. Nat Photonics 2007;1:336–42. https://doi.org/10.1038/nphoton.2007.76.
[32] Altarelli M, Brinkmann R, Chergui M, Decking W, Dobson B, Düsterer S, et al. The European X-ray free-electron laser. Gemeinsamer Bibliotheksverbund ISBN: Technical design report; 2007.
[33] Decking W, Abeghyan S, Abramian P, Abramsky A, Aguirre A, Albrecht C, et al. A MHz-repetition-rate hard X-ray free-electron laser driven by a superconducting linear accelerator. Nat Photonics 2020;14:391–7. https://doi.org/10.1038/s41566-020-0607-z.
[34] Stephan F, Boulware CH, Krasilnikov M, Bähr J, Asova G, Donat A, et al. Detailed characterization of electron sources yielding first demonstration of European X-ray Free-Electron Laser beam quality. Phys Rev ST Accel Beams 2010;13:020704. https://doi.org/10.1103/PhysRevSTAB.13.020704.
[35] Krasilnikov M, Stephan F, Asova G, Grabosch H-J, Groß M, Hakobyan L, et al. Experimentally minimized beam emittance from an L-band photoinjector. Phys Rev ST Accel Beams 2012;15:100701. https://doi.org/10.1103/PhysRevSTAB.15.100701.
[36] I. Isaev Stability and Performance Studies of the PITZ Photoelectron Gun 2017 Universität Hamburg.
[37] Ruan J-L, Lee C, Wouters S, Tullis IDC, Verslegers M, Mysara M, et al. Irradiation at ultra-high (FLASH) dose rates reduces acute normal tissue toxicity in the mouse gastrointestinal system. Int J Radiat Oncol Biol Phys 2021;111:1250–61. https://doi.org/10.1016/j.ijrobp.2021.08.004.
[38] Vozenin M-C, Montay-Gruel P, Limoli C, Germond J-F. All irradiations that are ultra-high dose rate may not be FLASH: The critical importance of beam parameter characterization and in vivo validation of the FLASH Effect. Radiat Res 2020;194: 571–2. https://doi.org/10.1667/rade-20-00141.1.
[39] Schüller A, Heinrich S, Fouillade C, Subiel A, De Marzi L, Romano F, et al. The european joint research project UHDpulse – Metrology for advanced radiotherapy using particle beams with ultra-high pulse dose rates. Physica Med 2020;80: 134–50. https://doi.org/10.1016/j.ejmp.2020.09.020.
[40] Whitmore L, Mackay RI, van Herk M, Jones JK, Jones RM. Focused VHEE (very high energy electron) beams and dose delivery for radiotherapy applications. Sci Rep 2021;11:14013. https://doi.org/10.1038/s41598-021-93276-8.
[41] Sanchez-Cano C, Alvarez-Puebla RA, Abendroth JM, Beck T, Blick R, Cao Y, et al. X-ray-based techniques to study the nano-bio interface. ACS Nano 2021;15: 3754–807. https://doi.org/10.1021/acsnano.0c09563.
[42] Körnig C, Staufer T, Schmutzler O, Bedke T, Machicote A, Liu B, et al. In-situ X-ray fluorescence imaging of the endogenous iodine distribution in murine thyroids. Sci Rep 2022;12:2903. https://doi.org/10.1038/s41598-022-06786-4.
[43] Grüner F, Blumendorf F, Schmutzler O, Staufer T, Bradbury M, Wiesner U, et al. Localising functionalised gold-nanoparticles in murine spinal cords by X-ray fluorescence imaging and background-reduction through spatial filtering for human-sized objects. Sci Rep 2018;8:16561. https://doi.org/10.1038/s41598-018-34925-3.
[44] Schmutzler O, Graf S, Behm N, Mansour WY, Blumendorf F, Staufer T, et al. X-ray fluorescence uptake measurement of functionalized gold nanoparticles in tumor cell microsamples. Int J Mol Sci 2021;22:3691. https://doi.org/10.3390/ijms22073691.
[45] Kahl H, Staufer T, Körnig C, Schmutzler O, Rothkamm K, Grüner F. Feasibility of monitoring tumor response by tracking nanoparticle-labelled T cells using X-ray fluorescence imaging—A numerical study. Int J Mol Sci 2021;22:8736. https://doi.org/10.3390/ijms22168736.
[46] Ungerer A, Staufer T, Schmutzler O, Körnig C, Rothkamm K, Gruener F. X-ray fluorescence imaging for in vivo detection of gold-nanoparticle-labeled immune cells: A GEANT4 based feasibility study. Cancers 2021;13:5759. https://doi.org/10.3390/cancers13225759.
[47] Flöttmann K. ASTRA particle tracking code, http://www.desy.de/~mpyflo/; 1997 [accessed 17 February 2022].
[48] Agapov I, Geloni G, Tomin S, Zagorodnov I. OCELOT: A software framework for synchrotron light source and FEL studies. Nucl Instrum Methods Phys Res, Sect A 2014;768:151–6. https://doi.org/10.1016/j.nima.2014.09.057.
[49] Agostinelli S, Allison J, Amako KA, Apostolakis J, Araujo H, Arce P, et al. GEANT4 - A simulation toolkit. Nucl Instrum Methods Phys Res, Sect A 2003;506:250–303. https://doi.org/10.1016/S0168-9002(03)01368-8.
[50] Obier F, Decking W, Hüning M, Wortmann J. Long pulse kicker for European XFEL beam distribution. FEL2019: Proceedings of the 39th Free Electron Laser Conference; 2019 Aug 26-30; Hamburg, Germany. p. 357-9. https://doi.org/10.18429/JACoW-FEL2019-WEP014.
[51] Loisch G, Agapov I, Antipov SA, Jebramcik MA, Keil J, Obier F. Stripline kickers for injection into PETRA IV. IPAC 2021: Proceedings of the 12th International Particle Accelerator Conference; 2021 May 24-28; Campinas, Brazil. p. 2863-5. https://doi.org/10.18429/JACoW-IPAC2021-WEPAB113.
[52] Lynch G, Dahl O. Approximations to multiple Coulomb scattering. Nucl Instrum Methods Phys Res, Sect B 1991;58:6–10. https://doi.org/10.1016/0168-583X(91)95671-Y.
[53] Issler L, Ruoß H, Häfele P. Festigkeitslehre-Grundlagen. 2nd ed. Berlin: Springer; 2005.

[54] National Institute of Standards and Technology, https://physics.nist.gov/PhysRefData/Star/Text/ESTAR.html; 2022 [accessed 30 March 2022].
[55] Ferrari A, Sala PR, Fassò A, Ranft J. FLUKA: A multi-particle transport code. CERN Yellow Reports: Monographs 2005. https://doi.org/10.2172/877507.
[56] Böhlen TT, Cerutti F, Chin MPW, Fassò A, Ferrari A, Ortega PG, et al. The FLUKA code: Developments and challenges for high energy and medical applications. Nucl Data Sheets 2014;120:211–4. https://doi.org/10.1016/j.nds. 2014.07.049.
[57] Esplen N, Mendonca MS, Bazalova-Carter M. Physics and biology of ultrahigh dose-rate (FLASH) radiotherapy: A topical review. Phys Med Biol 2020;65:23TR03. https://doi.org/10.1088/1361-6560/abaa28.
[58] Ashraf MR, Rahman M, Zhang R, Williams BB, Gladstone DJ, Pogue BW, et al. Dosimetry for FLASH radiotherapy: A review of tools and the role of radioluminescence and cherenkov emission. Front Phys 2020;8:328. https://doi.org/10.3389/fphy.2020.00328.
[59] Kokurewicz K, Schüller A, Brunetti E, Subiel A, Kranzer R, Hackel T, et al. Dosimetry for new radiation therapy approaches using high energy electron accelerators. Front Phys 2020;8:568302. https://doi.org/10.3389/fphy.2020.568302.
[60] IBA Dosimetry, https://www.iba-dosimetry.com; 2022 [accessed 21 February 2022].
[61] PTW Dosimetry, https://www.ptwdosimetry.com/en/; 2022 [accessed 21 February 2022].
[62] Ashland, https://www.ashland.com/file_source/Ashland/Documents/PHA21-011_Gafchromic%20EBT-XD%20Protocol.pdf; 2022 [accessed 6 September 2022].
[63] Proceedings of the Sixty-Seventh Annual Scientific Meeting of Canadian Organization of Medical Physicists; 2021 June 22-25; Virtual Event. Med. Phys. 2021;48:4657-710. https://doi.org/10.1002/mp.15102.
[64] Subiel A. FLASH in the Clinic Track FLASH RT: Current status of dosimetry, QA, challenges and the need for further developments. Physica Med 2022;94:S2. https://doi.org/10.1016/S1120-1797(22)01443-0.
[65] Lee N, Lourenco A, Thomas R, Romano F, Palmans H, Lee E, et al. FLASH modalities Track (Oral Presentations) development and test of a small portable graphite calorimeter for use in ultra-high dose rate particle beams. Physica Med 2022;94:S23. https://doi.org/10.1016/S1120-1797(22)01482-X.
[66] Di Martino F, Barca P, Barone S, Bortoli E, Borgheresi R, De Stefano S, et al. FLASH radiotherapy with electrons: Issues related to the production, monitoring, and dosimetric characterization of the beam. Front Phys 2020;8:570697. https://doi.org/10.3389/fphy.2020.570697.
[67] Gómez F, Gonzalez-Castaño DM, Gómez Fernández N, Pardo-Montero J, Schüller A, Gasparinihttps A, et al. Development of an ultra-thin parallel plate ionization chamber for dosimetry in FLASH radiotherapy. Med Phys 2022;49:4705–14. https://doi.org/10.1002/mp.15668.
[68] McManus M, Romano F, Lee ND, Farabolini W, Gilardi A, Royle G, et al. The challenge of ionisation chamber dosimetry in ultra-short pulsed high dose-rate very high energy electron beams. Sci Rep 2020;10:9089. https://doi.org/10.1038/s41598-020-65819-y.
[69] Berdalovic I, Argemi LS, Cardella R, Dachs F, Dao V, Sanz de Acedo LF, et al. MALTA: a CMOS pixel sensor with asynchronous readout for the ATLAS High-Luminosity upgrade. Proceedings of the 2018 IEEE Nuclear Science Symposium and Medical Imaging Conference Proceedings (NSS/MIC); 2018 Nov 10-17; Sydney, Australia. p. 1-4. https://doi.org/10.1109/NSSMIC.2018.8824349.
[70] Benhammadi S, Dopke J, Guerrini N, Phillips P, Sedgwick I, Villani G, et al. DECAL: A Reconfigurable Monolithic Active Pixel Sensor for use in Calorimetry and Tracking. TWEPP2019: Proceedings of Topical Workshop on Electronics for Particle Physics; 2019 Sep 2-6; Santiago de Compostela, Spain. p. 040. https://doi.org/10.22323/1.370.0040.
[71] Ballabriga R, Campbell M, Llopart X. An introduction to the Medipix family ASICs. Radiat Meas 2020;136:106271. https://doi.org/10.1016/j.radmeas.2020.106271.
[72] Advacam, https://advacam.com; 2022 [accessed 24 February 2022].
[73] ECFA Detector R&D Roadmap Process Group. The 2021 ECFA detector research and development roadmap. Geneva: CERN; 2020. https://doi.org/10.17181/CERN.XDPL.W2EX.
[74] U.S. Department of Energy, https://science.osti.gov/hep/Community-Resources/Reports; 2022 [accessed 6 September 2022].
[75] BRN Study, http://doe-brn-hep-detectorrandd.physics.ox.ac.uk/; 2019 [accessed 6 September 2022].